Available online at www.sciencedirect.com
ScienceDirect
Thermochimica Acta 467 (2008) 20–29
thermochimica acta
www.elsevier.com/locate/tca

The investigation of thermal decomposition pathways of phenylalanine and tyrosine by TG–FTIR

Li Jie [a], Liu Yuwen [a,b,*], Shi Jingyan [a], Wang Zhiyong [a], Hu Ling [a], Yang Xi [a], Wang Cunxin [a]

[a] College of Chemistry and Molecular Sciences, Wuhan University, Wuhan 430072, Hubei, China
[b] College of Life Sciences, Wuhan University, Wuhan 430072, Hubei, China

Received 13 February 2007; received in revised form 15 October 2007; accepted 24 October 2007
Available online 4 November 2007

Abstract

An online-coupled TG–FTIR evolved gas analysis (EGA) instruments have been used to identify and monitor the evolution of gaseous products during the thermal decomposition of phenylalanine and tyrosine in flowing N_2 atmosphere up to 800 °C. The results indicate that the thermolysis processes of these two compounds are similar. For both of them the main primary decomposition steps are two competing paths: the direct decarboxylation and the concerted rupturing of C–C bonds. And the primary decomposition reactions also include deamination and dehydration. The main secondary reaction is the crack of cyclic dipeptide which also presents two competing pathways. The main gaseous products are NH_3, H_2O, CO_2, CO, HNCO, HCN and some organic compounds. However, compared with tyrosine, the decomposition of phenylalanine is more complete and involves less secondary reaction. That is caused by their different thermal stability and decomposition temperature.

Keywords: TG–FTIR; Thermal decomposition; Phenylalanine; Tyrosine

1. Introduction

Most of biomass fuels, such as bagasse, straw, rapeseed and wood, contain nitrogen. Although the nitrogen content in biomass fuels is low, it is still important since the biomass nitrogen can be transformed into environmentally harmful gases under combustion and coking. It was found that most of the nitrogen in biomass fuels comes from proteins. The main pyrolytic gases from protein at high temperatures are HCN, NH_3 and HNCO. And their yields depend on temperature and also on the protein's amino acid composition [1]. Then the investigation of the pyrolysis of amino acid can bring us helpful information about the gaseous products released from protein and biomass fuels.

The pyrolysis of amino acid has been extensively studied in the last two decades [2–19]. Many techniques, such as UV [15,17], IR [4,6,9], Raman [9], NMR [4,18], HPLC [14,15,17], GC–MS [2,4,5,7,16,18,19], GC–FTIR–MS [14,17], TG [18], DSC [10] and TG–DSC [11,12,13] have been used to identify the products and mechanisms of their thermal decomposition. Now it is well known that their decomposition products include simple inorganic compounds (CO_2, H_2O, NH_3 and CO), with a variety of volatile organic compounds (amines, nitriles, amides, hydrocarbons, etc.) and lots of less-volatile organic compounds (2,5-piperazinediones, lactams, hydantoins, etc.). And the thermal fragmentations of various amino acids are considered as very complicated processes, which involved many pathways such as decarboxylation, deamination, dehydration and a number of intermolecular condensation reactions [14]. However, the thermal decomposition pathways of the amino acid cannot be interpreted clearly, and many reaction mechanisms remain uncertain [4,5,11,12,14,18].

Recently, we have studied the solid-state decomposition processes of some aliphatic amino acids in flowing N_2 atmosphere by TG–FTIR [20,21]. This paper is focused on determination of the thermal decomposition reaction sequences of two aromatic amino acid, phenylalanine and tyrosine, in the inert atmosphere.

* Corresponding author at: College of Chemistry and Molecular Sciences, Wuhan University, Wuhan 430072, Hubei, China. Fax: +86 27 68754067.
E-mail address: ipc@whu.edu.cn (L. Yuwen).

0040-6031/$ – see front matter © 2007 Elsevier B.V. All rights reserved.
doi:10.1016/j.tca.2007.10.014

These two compounds have similar molecular structure. The only difference between them is that tyrosine has a phenolic hydroxyl group more than phenylalanine.

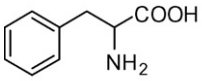

L-phenylalanine

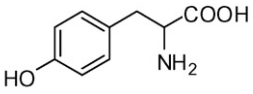

L-tyrosine

In previous studies of thermal decomposition mechanism of amino acid, almost all investigations were based upon off-line products detection [2–19]. By such methods, all products from different reaction steps were mixed together, which brought many troubles to identify the sequences of the reactions occurred. To give more details of thermal induced behavior, an on-line monitoring method is needed. In present work, the TG–FTIR technique, which can conduct simultaneous and continuous real time analysis [22–26] was used. And more specific information about the sequence of reaction steps and the relevant quantity of gaseous products can be obtained.

2. Theoretical

In present work, a semi-quantitative method was used to determine the components of the gaseous mixtures (in following description, two components are assumed) by IR absorbance spectrum.

First, several wave numbers are selected for the characteristic IR absorbance of this two components. From the standard IR spectrum of the two components, the IR absorbance (A_{ij}) at these wave numbers are gotten, respectively:

$$\text{component 1 } (i=1): \quad A_{11}, A_{12}, A_{13}, A_{14}, \ldots$$
$$\text{component 2 } (i=2): \quad A_{21}, A_{22}, A_{23}, A_{24}, \ldots$$

Second, according to Lambert–Beer Law, a function can be constructed as follows:

$$A = \varepsilon c l$$

where A is the IR absorbance, ε is the absorption coefficient, c is the concentration of this component and l is the light path length. For the same standard spectrum, both c and l are constant. Then when it is assumed that the maximum of A_{1j} (j = 1, 2, 3, 4,...) is A_M and the maximum of A_{2j} (j = 1, 2, 3, 4,...) is A_N, and the corresponding absorption coefficients are ε_M and ε_N, one can obtain:

$$\text{component 1}: \quad k_{11} = \frac{A_{11}}{A_M} = \frac{\varepsilon_{11}}{\varepsilon_M}, \quad k_{12} = \frac{A_{12}}{A_M} = \frac{\varepsilon_{12}}{\varepsilon_M}, \quad k_{13} = \frac{A_{13}}{A_M} = \frac{\varepsilon_{13}}{\varepsilon_M}, \quad k_{14} = \frac{A_{14}}{A_M} = \frac{\varepsilon_{14}}{\varepsilon_M}, \ldots$$
$$\text{component 2}: \quad k_{21} = \frac{A_{21}}{A_N} = \frac{\varepsilon_{21}}{\varepsilon_N}, \quad k_{22} = \frac{A_{22}}{A_N} = \frac{\varepsilon_{22}}{\varepsilon_N}, \quad k_{23} = \frac{A_{23}}{A_N} = \frac{\varepsilon_{23}}{\varepsilon_N}, \quad k_{24} = \frac{A_{24}}{A_N} = \frac{\varepsilon_{24}}{\varepsilon_N}, \ldots$$

Third, in the IR spectrum of the mixtures the absorbance intensity at these selected wave numbers can be described as follows:

$$A_j = \varepsilon_{1j} c_1 l + \varepsilon_{2j} c_2 l$$
$$= k_{1j} c_1 \varepsilon_M l + k_{2j} c_2 \varepsilon_N l \quad (j = 1, 2, 3, 4, \ldots)$$

If we assume $c_1 \varepsilon_M l = c_1'$, $c_2 \varepsilon_N l = c_2'$ we can get $A_j = k_{1j} c_1' + k_{2j} c_2'$. Then a linear function group is obtained, by which the values of c_1' and c_2' can be determined. Because the values of ε_M and ε_N are determined by the species of the components, and l is the instrument

$$\begin{bmatrix} k_{11} & k_{21} \\ k_{12} & k_{22} \\ k_{13} & k_{23} \\ k_{14} & k_{24} \\ \cdots & \end{bmatrix} \times \begin{bmatrix} c_1' \\ c_2' \end{bmatrix} = \begin{bmatrix} A_1 \\ A_2 \\ A_3 \\ A_4 \\ \cdots \end{bmatrix}$$

constant, the values of c_1' and c_2' can represent the concentration of the components. And the change of the values of c_1' and c_2' can reveal the concentration changes of the components 1 and 2, respectively. But it should be noted that it is meaningless to compare the value of c_1' with that of c_2', for they include different absorption coefficients. Another noticeable thing is that the value of k_{ij} can be impacted by the experimental condition. Then the difference between the experimental condition in which the standard spectra were obtained and that in which the spectra of the mixtures were obtained will affect the accuracy of calculation.

3. Experiment

Commercially available phenylalanine and tyrosine (Analytical Grade, purchased from Wako, Japan) were used without further purification.

The TG–FTIR system composed of a Setaram Setsys 16 TG-DTA/DSC Instrument and a Thermo Nicolet Nexus 670 Fourier Transform Infrared Spectrometer. For TG–FTIR measuring, about 10 mg sample was weighted into an open alumina crucible. The heating rate of the TG furnace was 20 °C min^{-1}, and nitrogen gas of high purity (>99.999%) with a flow rate of 100 ml min^{-1} was used as carrier gas. The sample was heated from ambient temperature to 800 °C. The transfer line used to connect TG and FTIR was a 1 m long stainless steel tube with an internal diameter of 2 mm, of which the temperature is maintained at 200 °C. The TGA accessory of the IR Spectrometer was used, which has a 45 ml gas cell with a 200 mm path length. It was also heated at the constant temperature of 200 °C. The IR spectra were collected at 8 cm^{-1} resolution, co-adding eight scans per spectrum. This resulted in a temporal resolution of 4.32 s. Lag time that the gas products went from furnace to gas cell was about 7 s. The FTIR spectra were identified based on the FTIR reference spectra available on the World Wide Web in the public spectrum libraries of NIST [27] and SADTLER Standard Infrared Spectra [28].

4. Results and discussion

4.1. Thermal decomposition of phenylalanine

Fig. 1 presents weight loss (TG), associated derivative thermogram (DTG) and total infrared absorbance (Gram–Schmidt

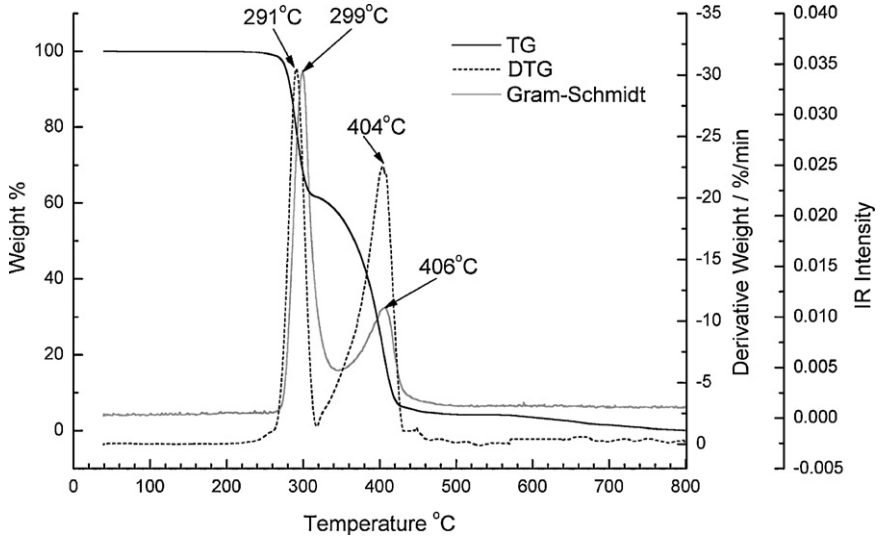

Fig. 1. The curves of TG, DTG and the total FTIR absorbance intensity of evolved gases gotten during the phenylalanine pyrolysis process by TG–FTIR (heating rate 20 °C min^{-1}; N_2 flow rate 100 ml min^{-1}).

curve) profiles of phenylalanine as the function of temperature. In this figure, the lag time of the evolved gases passing through the IR cell has been subtracted. TG curve shows two distinct weight loss stages. The first stage occurs in the temperature range of 242–317 °C with a sharp weight loss of 38.3%. The second stage occurs in the temperature range of 317–452 °C with a weight loss of 57.4%. After that the phenylalanine keeps slow weight losing, the total weight loss at 800 °C is almost 100%. Comparison of Gram–Schmidt curve with DTG curve indicates that the temperature of IR absorbance peaks coincide with that of DTG peaks. Gram–Schmidt curve shows two peaks existing at 299 and 406 °C, and the DTG curve shows two peaks at 291 and 404 °C.

The 3D FTIR spectrum of the evolved gases of phenylalanine pyrolysis is shown in Fig. 2. In this figure, FTIR spectrum of all the volatile pyrolysis products produced at different time are shown. And the characteristic spectra obtained at 299, 346, 406 and 424 °C are shown in Fig. 3. From Fig. 3, eight small molecular gaseous species are easily identified by

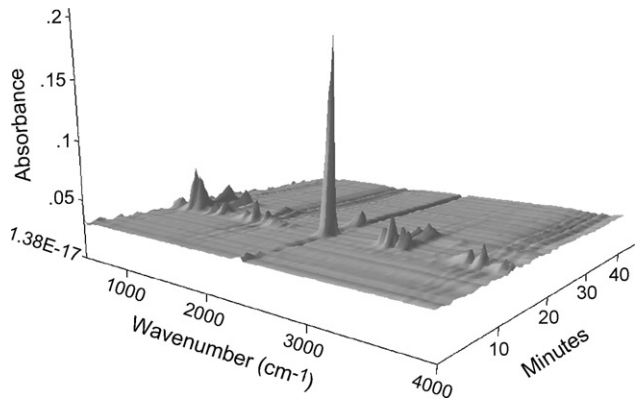

Fig. 2. The 3D surface graph for the FTIR spectra of the evolved gases produced by phenylalanine pyrolysis (heating rate 20 °C min^{-1}; N_2 flow rate 100 ml min^{-1}).

their characteristic absorbance: CO_2 ($\nu_{C=O}$ 2358 cm^{-1}); NH_3 (δ_{N-H} 965, 930 cm^{-1}); H_2O (ν_{O-H} 3400–4000 cm^{-1}, δ_{O-H} 1300–1900 cm^{-1}); CO ($\nu_{C=O}$ 2181, 2112 cm^{-1}); HNCO ($\nu_{C=N}$ 2250 cm^{-1}, $\nu_{C=O}$ 2280 cm^{-1}); HCN (ν_{C-H} 3330, 3270 cm^{-1}, δ_{C-H} 713 cm^{-1}); benzeneethanamine ($\nu_{=C-H}$ 3079, 3036, ν_{C-H} 2933, 2859 cm^{-1}, $\nu_{C=C}$ 1606, 1493 cm^{-1}, $\delta_{=C-H}$ 1070, 1031 cm^{-1}, $\gamma_{=C-H}$ 741, 690 cm^{-1}); toluene ($\nu_{=C-H}$ 3071, 3032, ν_{C-H} 2933, 2868 cm^{-1}, $\nu_{C=C}$ 1598, 1498 cm^{-1}, $\gamma_{=C-H}$ 728, 695 cm^{-1}). Due to the lack of standard infrared spectrum for HNCO, we identified this species by comparing the spectra with the HNCO vapor phase spectrum from literatures [1,29].

Fig. 4 gives the evolution curves of all species of evolved gases. In this figure the evolution curves of all the species except H_2O are shown as the IR absorbance at characteristic wave numbers versus temperature. The evolution curve of H_2O is shown as the integral area in the range of 3776–4000 cm^{-1} versus temperature to avoid interference of the absorbance of other species. And because the characteristic infrared absorbance of benzeneethanamine and toluene partially overlaps, the curves of benzeneethanamine and toluene in Fig. 4 were obtained by the semi-quantitative calculation mentioned above with the IR absorbance at four characteristic wave numbers: 3079, 3036, 2933 and 2859 cm^{-1}.

Fig. 4 indicates that the pyrolysis process of phenylalanine is complicated. In the first stage main gaseous products are CO_2, NH_3, H_2O and benzeneethanamine. And from Figs. 2 and 3 it can be seen that in this stage the characteristic absorbance of CO_2 is far stronger than that of NH_3 and H_2O. Then we believe that in this stage the yield of CO_2 is higher than that of NH_3 and H_2O, considering that the IR absorption coefficients of these three species are not very different. This suggests that the main primary decomposition step of phenylalanine is decarboxylation which produces CO_2 and benzeneethanamine, dehydration and deam-

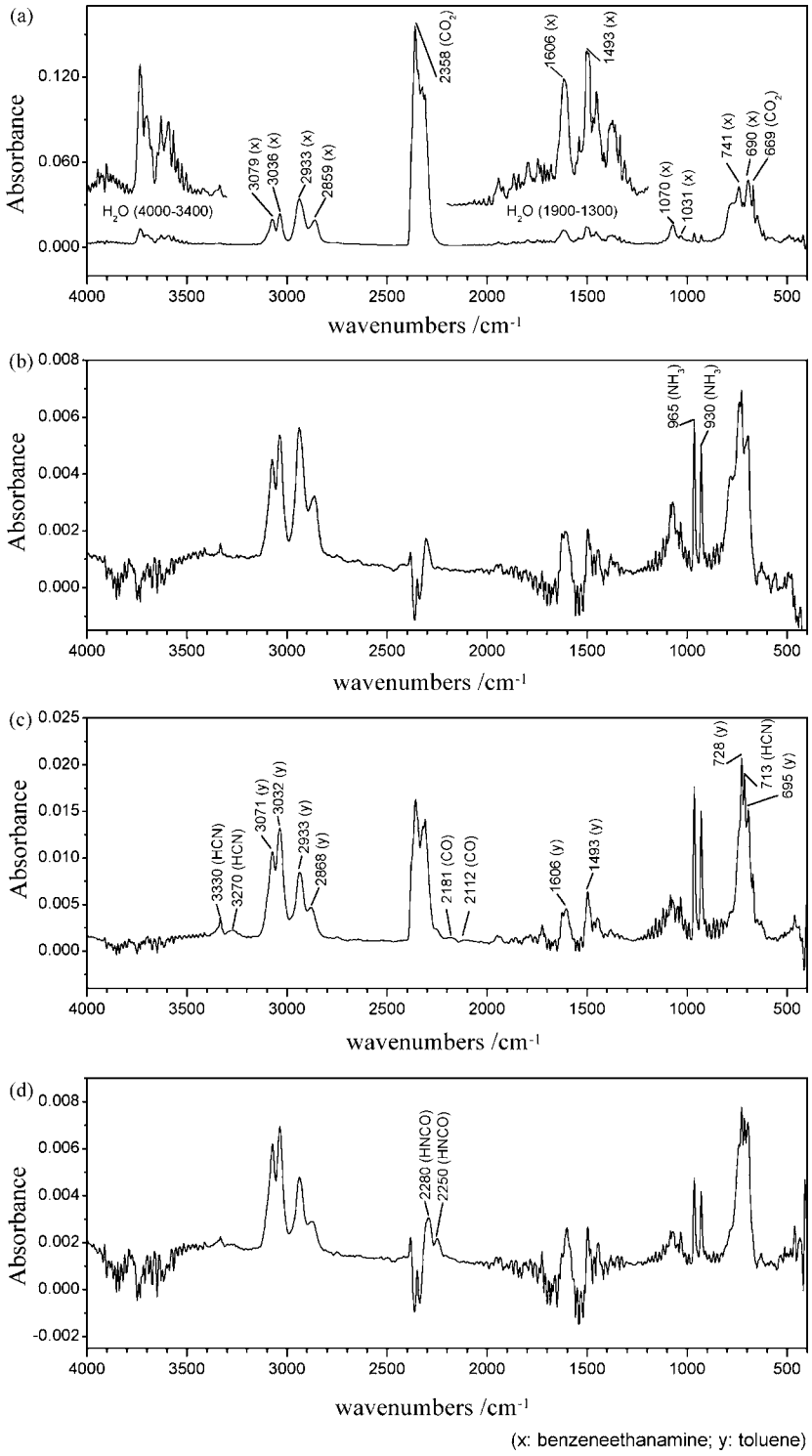

Fig. 3. The FTIR spectra of evolved gases from phenylalanine decomposed in N_2 measured at different temperature by online-coupled TG–FTIR (heating rate 20 °C min^{-1}; N_2 flow rate 100 ml min^{-1}): (a) at 299 °C; (b) at 346 °C; (c) at 406 °C; (d) at 424 °C.

ination is minor. That the absorbance of benzeneethanamine was detected in our experiment also supports this opinion.

In the second stage the gaseous products include NH_3, toluene, HNCO, HCN, CO and CO_2. Toluene instead of benzeneethanamine becomes the main organic product in this stage. And the formation of toluene takes place also accompanied by the formation of CO_2. It seems that decarboxylation occurs through two competing pathways: one is direct decarboxylation which produces bezeneethanamine and the other is the concerted rupturing of carbon chain which produces toluene. And in our experiment the decomposition temperature showed

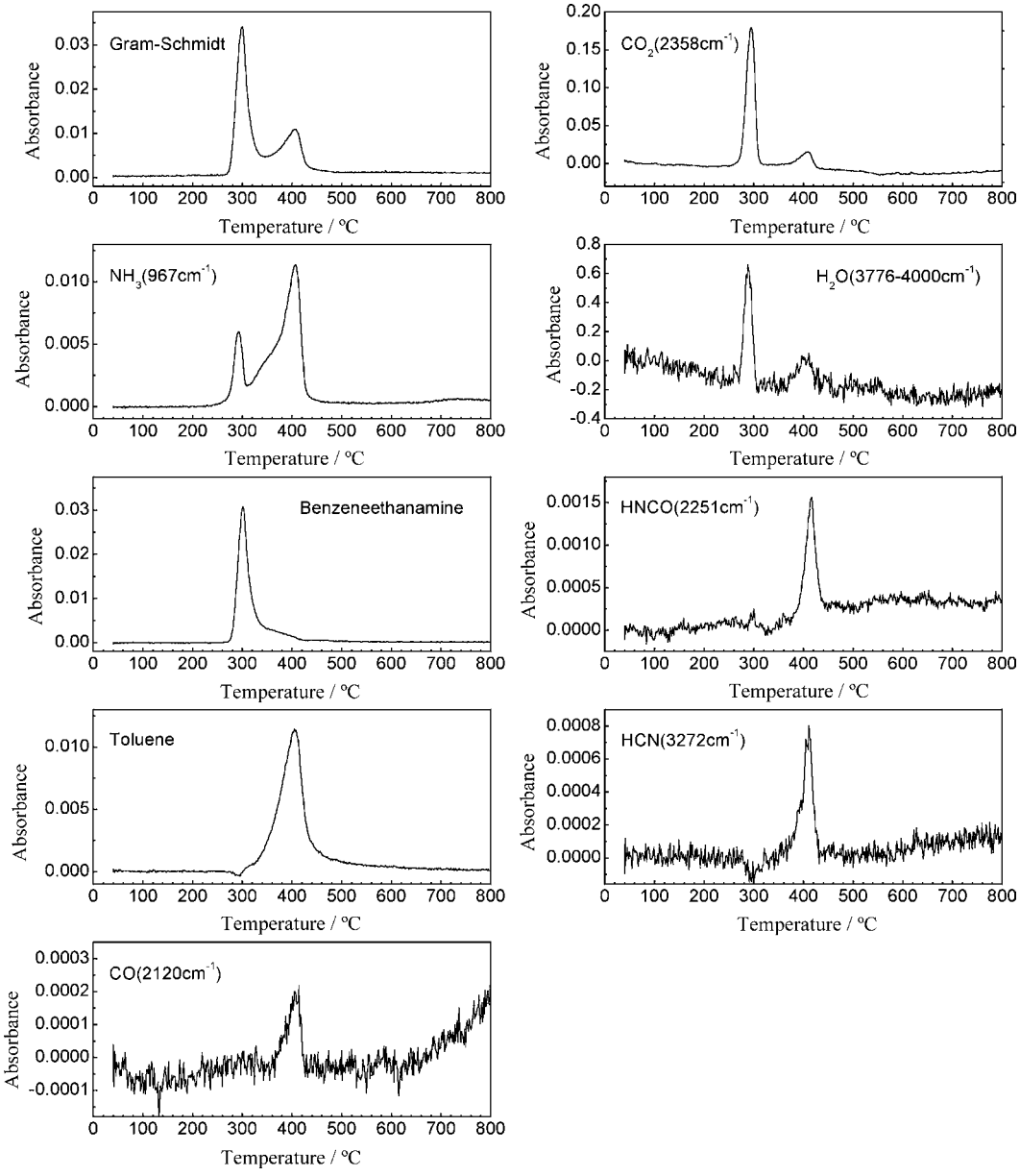

Fig. 4. IR absorbance vs. temperature curves of identified evolved gaseous species evolved from phenylalanine decomposed in N_2, measured by online-coupled TG–FTIR system (heating rate 20 °C min^{-1}; N_2 flow rate 100 ml min^{-1}).

great influence on the proportion between these two pathways. At low temperature the decarboxylation is the main pathway. And with increasing of the temperature, concerted rupturing of C–C bonds occurs to a greater extent in phenylalanine pyrolysis and participation of the decarboxylation intermediate, benzeneethanamine, becomes less important. As we know, amino acids will undergo a facile radical-catalyzed decarboxylation when heated [30]. Patterson suggested that in fast pyrolysis phenylalanine is decomposed by two competing paths: one involving decarboxylation followed by decomposition of the benzeneethanamine or its radical precursor (Eq. (1)) and the other involving a concerted or nearly concerted rupturing of bonds at positions a and b (Eq. (2)), which produced benzyl radical [6,31,32]. Our results indicate that in slow pyrolysis phenylalanine also decomposes by these two competing pathways.

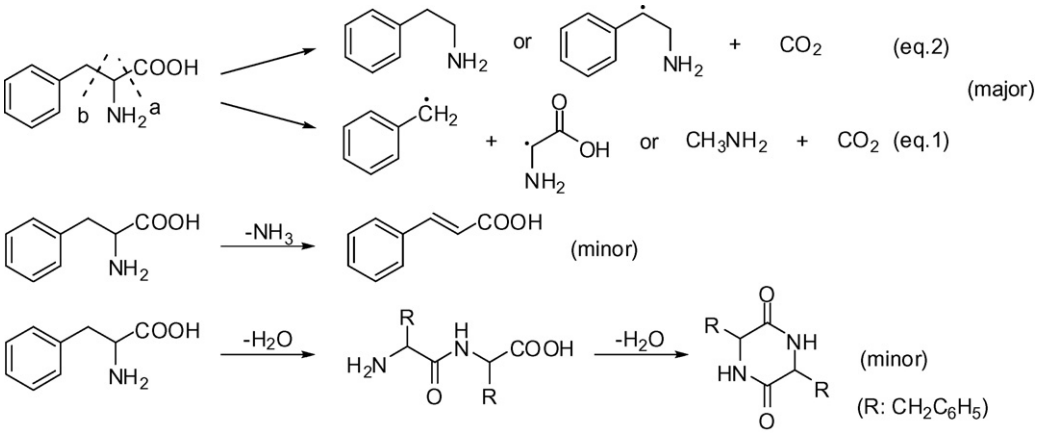

Dehydration mainly produces dipeptide, cyclic dipeptide (DKP) and polypeptides. The peptide forming reactions occur readily because they are simple dehydrations. And in the pyrolysis of amino acids, the thermal conditions provide sufficient energy to form intermediate peptides [18].

NH_3 can be formed from individual molecular reaction of phenylalanine. But it may also be formed as a result of the secondary reactions [4]. Both the decomposition reaction of primary amines and the bimolecular reactions between imine and amine can produce NH_3 [5]. The rapid releasing rate of NH_3 in the first stage reveals that individual molecular reaction is the main pathway of NH_3 formation. And NH_3 in the second stage may be produced in the secondary reactions.

The intermediate, 2,5-piperazinedione (DKP), can provide an attractive explanation for the formation of HNCO, HCN and CO. And HNCO also decomposes into HCN and CO in substantial pyrolysis step [33].

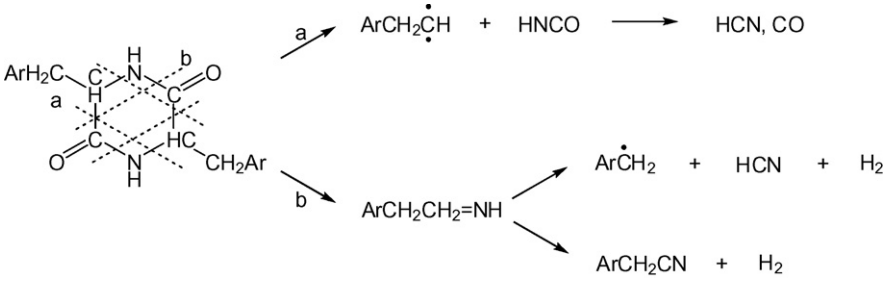

Hansson has suggested that in the process of protein pyrolysis HNCO and HCN are mainly formed from cracking of cyclic amides and the selectivity toward formation of HCN over the formation of HNCO is increased with the increase of temperature [1]. In the process of glycine and its dipeptide pyrolysis HNCO was observed to reach its maximum releasing rate at 400 °C and HCN reached its maximum releasing rate at 700 °C [21]. However, Fig. 4 indicates that in the process of phenylalanine pyrolysis HNCO and HCN were produced simultaneously around 400 °C. We believe that that is caused by the low yield of DKP from phenylalanine. Because dehydration contributes to the formation of DKP, the low yield of H_2O predicates the low yield of DKP. And the small quantity of DKP will decompose completely at 440 °C. So the changes in ratio of HNCO/HCN cannot be observed in our experiment.

4.2. The thermal decomposition of tyrosine

The weight loss, the associated derivative thermogram and the total infrared absorbance profile of the tyrosine are shown in Fig. 5. Although tyrosine has similar molecular structure as phenylalanine, the thermal decomposition process of tyrosine is markedly different from that of phenylalanine. Three weight loss stages can be found in the TG curve of tyrosine. Like phenylalanine, the first weight loss stage of tyrosine pyrolysis is sharp, and takes place in a higher temperature range of 306–347 °C with weight loss of 40%. This indicates that tyrosine has higher thermal stability than phenylalanine. The second stage (347–431 °C) and the third stage (431–800 °C) overlap partially. And compared with phenylalanine, the pyrolysis of tyrosine produces more solid residua. The overall weight loss at 800 °C is only 80.6%. DTG curve and Gram–Schmidt curve are correlated with the weight loss observed in TG trace.

Fig. 6 is 3D FTIR spectrum of evolved gases of tyrosine pyrolysis, and Fig. 7shows the characteristic spectra obtained at 334, 345, 378 and 635 °C. From them, eight gaseous species are easily identified by their characteristic absorbance. Besides CO_2, NH_3, CO, HCN and H_2O which were also detected in phenylalanine pyrolysis, other three species were detected: CH_4 ($\nu_{C–H}$ 3016 cm^{-1}, $\delta_{C–H}$ 1303 cm^{-1}); 4-methylphenol ($\nu_{O–H}$ 3649 cm^{-1}, $\nu_{C–H}$ 3026, 2936, 2880 cm^{-1}, $\nu_{C=C}$ 1611, 1514 cm^{-1}, $\nu_{C–O}$ 1254 cm^{-1}, $\delta_{O–H}$ 1175 cm^{-1}, $\delta_{C–H}$ 817 cm^{-1}); phenol ($\nu_{O–H}$ 3649 cm^{-1}, $\nu_{C–H}$ 3057 cm^{-1}, $\nu_{C=C}$ 1611, 1514 cm^{-1}, $\nu_{C–O}$ 1254 cm^{-1}, $\delta_{O–H}$ 1175 cm^{-1}, $\delta_{C–H}$ 748, 684 cm^{-1}). The quantity changes of all species

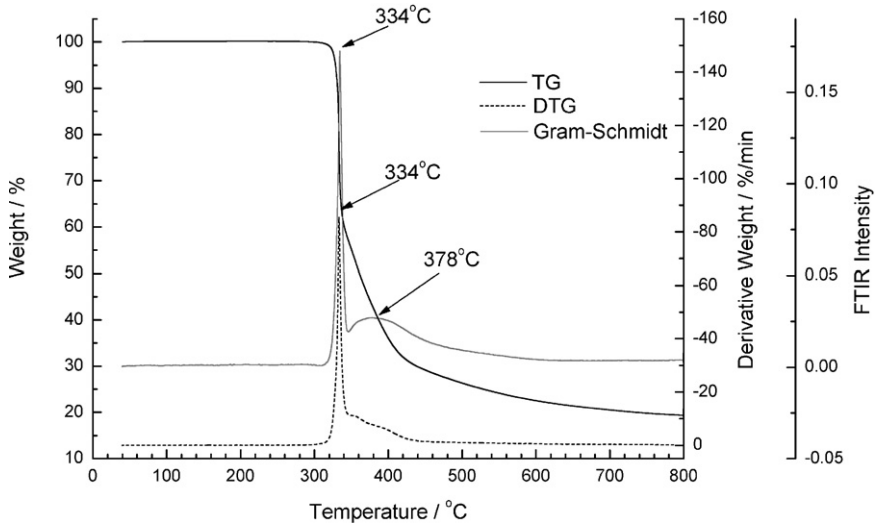

Fig. 5. The curves of TG, DTG and the total FTIR absorbance intensity of evolved gases, gotten during the tyrosine pyrolysis process by TG–FTIR (heating rate 20 °C min^{-1}, N_2 flow rate 100 ml min^{-1}).

versus temperature are shown in Fig. 8, of which the releasing curves of 4-methylphenol and phenol are obtained by the semi-quantitative calculation according to the IR absorbance at seven wave numbers: 3029, 2936, 2882, 1603, 1511, 817 and 748 cm^{-1}.

Fig. 8 shows that the main gaseous products are CO_2, NH_3 and H_2O in the first stage of the tyrosine decomposition, and the yield of CO_2 is larger than the other two. It indicates that the primary decomposition steps of tyrosine include decarboxylation, deamination and dehydration, in which the decarboxylation is the main reaction. This is the same as that in the thermal decomposition of phenylalanine. The tyrosine decarboxylation will produce 4-(2-aminoethyl)phenol and CO_2. However, no 4-(2-aminoethyl)phenol can be detected in our experiment due to its low volatility.

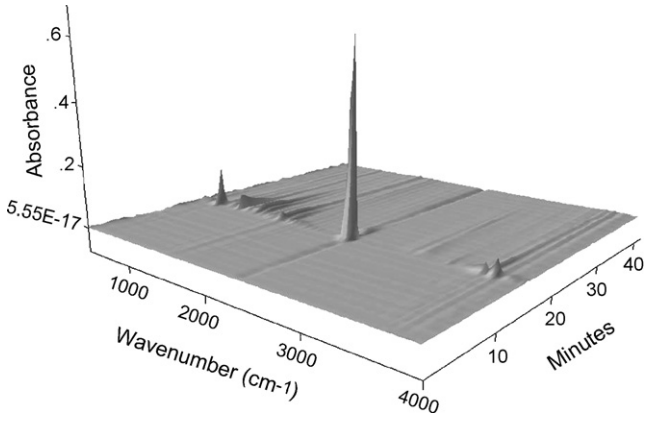

Fig. 6. The 3D surface graph for the FTIR spectra of the evolved gases produced by tyrosine pyrolysis (heating rate 20 °C min^{-1}; N_2 flow rate 100 ml min^{-1}).

In the second stage the gaseous products include 4-methylphenol, phenol, NH_3, HCN and CO. The 4-methylphenol can yield from tyrosine also by the concerted rupturing of C–C bonds. This indicates that the tyrosine decomposes also by two competing pathways as phenylalanine does. And Figs. 4 and 8 show that the formation of 4-methylphenol occurs at the same temperature range as the formation of toluene from phenylalanine does. The formation of phenol is probably the result of the further decomposing of 4-methylphenolic radical. Although no HNCO was detected in our experiment, the existence of CO, HCN and the dehydration reaction indicates the formation of DKP intermediate in tyrosine decomposition.

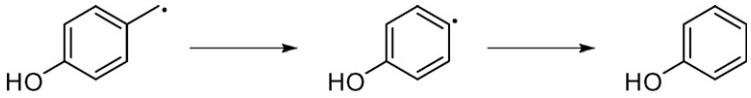

HCN, CO and CH_4 are the main gaseous products in the third stage. At 600 °C the max. releasing rate of CH_4 is reached. And the max. releasing rate of HCN is reached at 700 °C. This supports that the formation of HCN increases with the increasing of temperature. Then the cracking of DKP intermediate can be used to interpret the formation of HCN and CO. In the process of tyrosine pyrolysis the temperature at which the cracking of DKP starts is high, so the yield of HNCO should be low. So no HNCO releasing was detected can be understood.

The phenolic hydroxyl group in tyrosine can increase intermolecular force by forming hydrogen bond. This contributes to its higher thermal stability than phenylalanine. So the tyrosine begins to decompose at higher temperature than phenylalanine. And the proportion of dehydration in the primary reactions will increase with the increasing of temperature. Then the tyrosine produces more condensate by dehydration than phenylalanine. So tyrosine produces more residua than phenylalanine when heated.

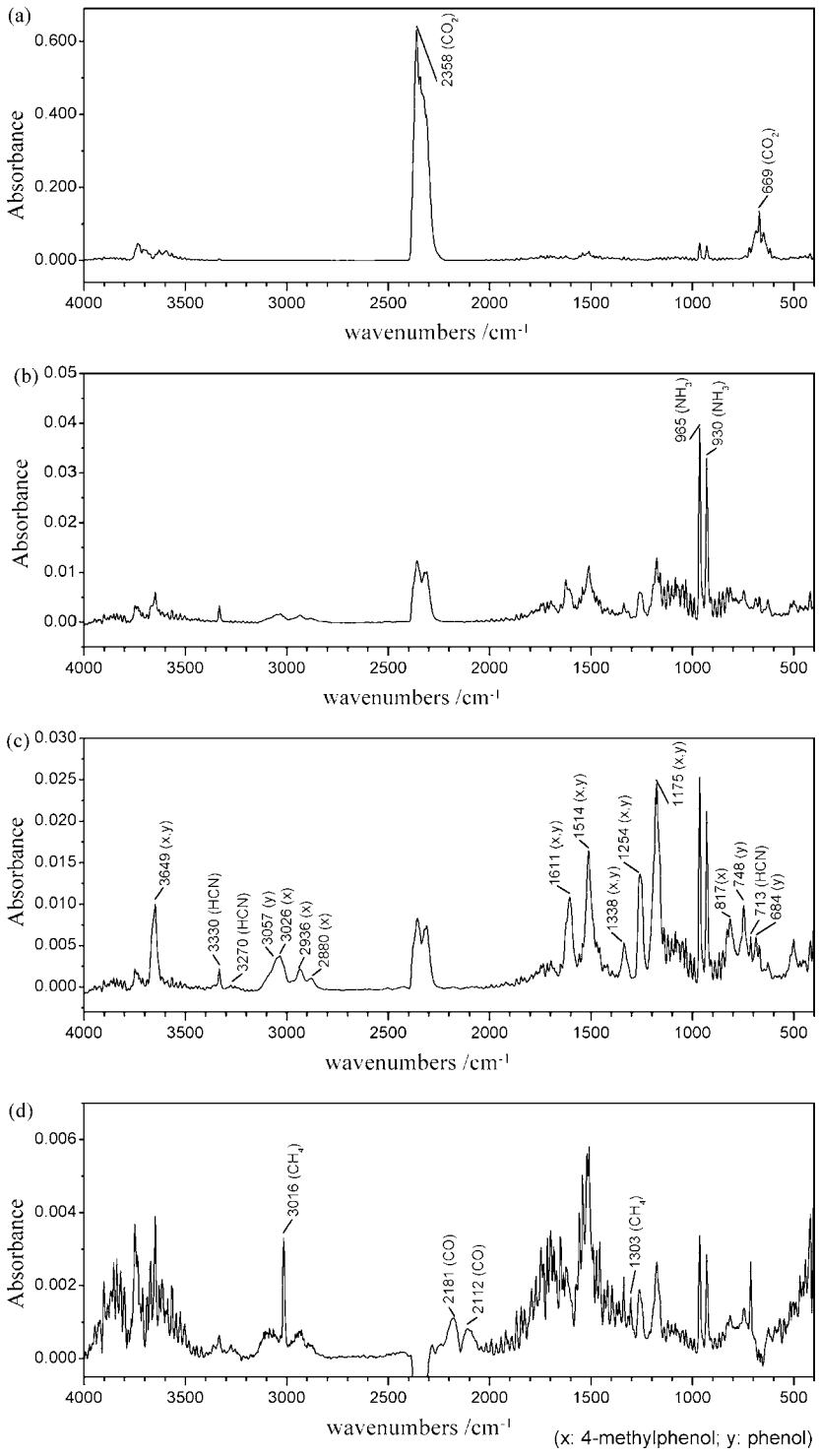

Fig. 7. The FTIR spectra of evolved gases from tyrosine decomposed in N_2 measured at different temperature by online-coupled TG–FTIR (heating rate 20 °C min^{-1}; N_2 flow rate 100 ml min^{-1}): (a) at 334 °C; (b) at 345 °C; (c) at 378 °C; (d) at 635 °C.

In the processes of glycine and its dipeptide pyrolysis HNCO and HCN was observed reaching their max. releasing rates at 400 and 700 °C, respectively [21]. Now in the processes of phenylalanine pyrolysis HNCO is observed reaching its max. releasing rates at 400 °C. And in the processes of tyrosine pyrolysis HCN is observed reaching its max. releasing rates at 700 °C. So we believe that in the processes of phenylalanine, tyrosine, glycine and its dipeptide pyrolysis, the formations of HNCO, HCN and CO occur though the same pathway.

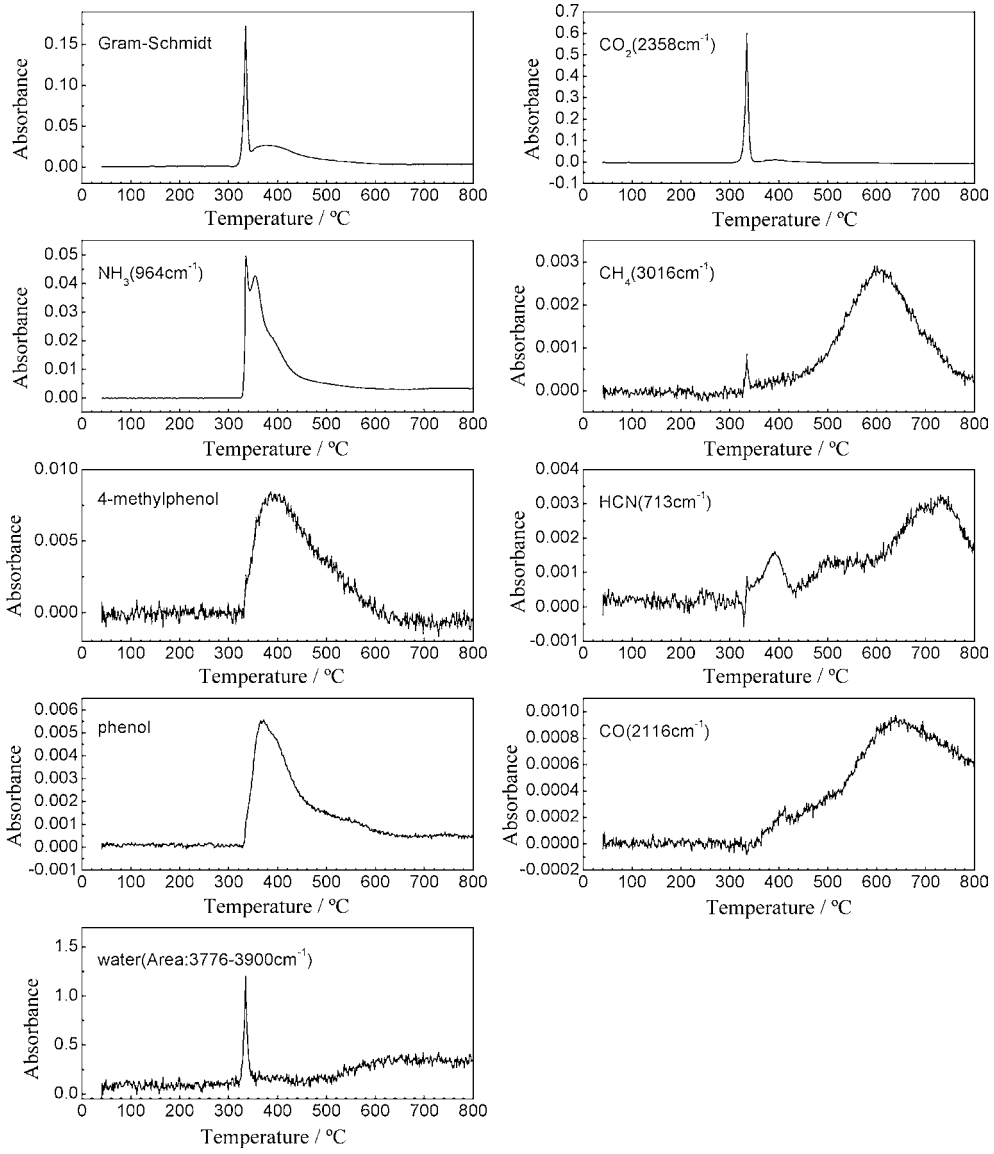

Fig. 8. IR absorbance vs. temperature curves of identified evolved gaseous species evolved from tyrosine decomposed in N_2, measured by online-coupled TG–FTIR system (heating rate 20 °C min^{-1}; N_2 flow rate 100 ml min^{-1}).

5. Conclusions

When heated under inert condition, the solid phenylalanine and tyrosine are decomposed through the similar processes. The processes are complicated, which include random bond cleavage, decarboxylation, deamination, dehydration and the crack of cyclic dipeptide. And the main gaseous products are NH_3, H_2O, CO_2, CO, HNCO, HCN and some small organic molecules. For both compounds the main primary decomposition steps are two competing paths: the random bond cleavage and the direct decarboxylation, and both paths can produce CO_2. At low temperature (<350 °C) the direct decarboxylation is major, and the concerted rupturing of C–C bonds become important with increasing of the temperature. And for both compounds the crack of cyclic dipeptide is also an important decomposition pathway which produces HNCO, HCN and CO. Compared with tyrosine, the decomposition of phenylalanine produce less solid residuum and harmful nitrogen containing gases, HNCO and HCN.

The TG–FTIR technique brings us more specific information about the gaseous products of pyrolysis online, such as the species of gaseous products, their quantities and evolution rate versus time. It supplies a comprehensive understanding of thermal events in a reliable and meaningful way as data are obtained from a single sample under the same conditions. And it is also a useful tool to determine the primary decomposition steps. Although it is difficult to identify every species in the mixture of gas products for the overlapping of their IR absorbance, some gas products with very specific IR absorption, such as CO_2, CO, H_2O and NH_3, can be identified easily.

Acknowledgements

This work was financially supported by the National Nature Sciences Foundation of China (Grant No. 20373050, and No. 30600116), Nature Sciences Foundation of Hubei and China Postdoctoral Science Foundation.

References

[1] K.M. Hansson, L.E. Amand, A. Habermann, F. Winter, Fuel 82 (2003) 653.
[2] C. Merritt, D.H. Robertson, J. Gas Chromatogr. 5 (1967) 96.
[3] W. Simon, P. Kriemler, H. Steiner, J. Gas Chromatogr. 5 (1967) 53.
[4] P.G. Simmonds, E.E. Medley, M.A. Ratcliff, G.P. Shulman, Anal. Chem. 44 (1972) 2060.
[5] M.A. Ratcliff, E.E. Medley, P.G. Simmonds, J. Org. Chem. 39 (1974) 1481.
[6] J.M. Patterson, N.F. Haidar, E.P. Papadopoulos, W.T. Smith, J. Org. Chem. 38 (1973) 663.
[7] G.P. Shulman, P.G. Simmonds, Chem. Commun. 15 (1968) 1040.
[8] N.D. Danielson, L.B. Rogers, Anal. Chem. 50 (1978) 1680.
[9] D. Bougeard, Ber. Bunsen. Phys. Chem. 87 (1983) 279.
[10] A. Grunenberg, D. Bougeard, B. Schrader, Thermochim. Acta 77 (1984) 59.
[11] F. Rodante, G. Marrosu, Thermochim. Acta 171 (1990) 15.
[12] F. Rodante, G. Marrosu, G. Catalani, Thermochim. Acta 194 (1992) 197.
[13] F. Rodante, Thermochim. Acta 200 (1992) 47.
[14] V.A. Basiuk, J. Anal. Appl. Pyrol. 47 (1998) 127.
[15] J. Douda, V.A. Basiuk, J. Anal. Appl. Pyrol. 56 (2000) 113.
[16] G. Chiavari, D. Fabbri, S. Prati, J. Chromatogr. A 922 (2001) 235.
[17] V.A. Basiuk, J. Douda, Adv. Space Res. 27 (2001) 231.
[18] R.K. Sharma, W. Geoffrey Chan, B.E. Jia Wang, J.B. Waymack, J.I. Wooten, M.R. Seeman, Hajaligol, J. Anal. Appl. Pyrol. 72 (2004) 153.
[19] S.F. Wang, B.Z. Liu, Q.D. Su, J. Anal. Appl. Pyrol. 71 (2004) 393.
[20] J. Li, Z. Wang, X. Yang, L. Hu, Y. Liu, C. Wang, Themochim. Acta 447 (2006) 147.
[21] J. Li, Z. Wang, X. Yang, L. Hu, Y. Liu, C. Wang, J. Anal. Appl. Pyrol. 80 (2007) 247.
[22] W. Xie, W.P. Pan, J. Therm. Anal. Calorim. 65 (2001) 669.
[23] K. Marsanich, F. Barontini, V. Cozzani, L. Petarca, Thermochim. Acta 390 (2002) 153.
[24] M. Webb, P.M. Last, C. Breen, Thermochim. Acta 326 (1999) 151.
[25] C. Breen, P.M. Last, S. Taylor, P. Komadel, Thermochim. Acta 363 (2000) 93.
[26] W.M. Groenewoud, W. de Jong, Thermochim. Acta 286 (1996) 341.
[27] NIST chemistry webbook standard reference database No. 69, June 2005 release (http://webbook.nist.gov/chemistry).
[28] SADTLER Standard Infrared Vapor Phase Spectra, Sadtler Research Laboratories, Inc., 1980.
[29] U. Eickhoff, F. Temps, Phys. Chem. Chem. Phys. 1 (1999) 243.
[30] G. Chatelus, Bull. Soc. Chim. Fr. (1964) 2523.
[31] W.R. Johnson, J.C. Kang, J. Org. Chem. 36 (1971) 189.
[32] N.F. Haidar, J.M. Patterson, M. Moors, W.T. Smith, J. Agric. Food Chem. 29 (1981) 165.
[33] R.A. Back, J. Childs, Can. J. Chem. 46 (1968) 1023.